

A study of reflection loss. I. A multilayered viscoelastic seabed at very low frequencies

A. C. Kibblewhite and C. Y. Wu

Department of Physics, University of Auckland, Private Bag 92019, Auckland, New Zealand

(Received 22 December 1993; accepted for publication 5 May 1994)

Recent investigations of wave-induced seismoacoustic noise in the ocean have involved a parallel study of the reflection coefficient of complex seabeds at very low frequencies. Because of the nature of the wave-wave interaction source responsible for the main peak in the ULF noise spectrum, it was necessary to examine the behavior of the reflection coefficient to both the homogeneous and inhomogeneous components of the wave-induced noise field. The results of these studies have revealed aspects of the reflection loss process not previously recognized. This contribution discusses the reflection loss for a multilayered viscoelastic structure. Companion papers examine the effect of introducing porosity into the sedimentary layers.

PACS numbers: 43.30.Ma, 43.30.Nb

INTRODUCTION

It is well known that the seafloor can significantly influence the propagation of sound in the ocean. Studies aimed at understanding the effects of bottom interaction have been an important part of underwater acoustics for many years and an extensive literature testifies to this fact. A traditional measure of acoustic interaction with the ocean bottom is bottom loss, which is characterized by the plane-wave reflection coefficient at the water-sediment interface, determined as a function of frequency and incident angle. For applications involving total energy processing in octave or third-octave bands this quantity has proved completely adequate. For other applications, however, a more detailed characterization on the seafloor has been required and the geoacoustic profile describing the depth dependence of key sediment properties has been invoked.

Determination of the reflection coefficient is obviously more complicated when the sediment properties are strongly depth dependent. In typical studies this depth dependence is often approximated by modeling the sediments as a number of homogeneous layers of different properties.^{1,2} In other analyses this approximation has been avoided by modeling the sediments as a fluid, the properties of which vary continuously with depth.³⁻⁵ Developments in the late 1970s considered a more realistic view of the sediment as a solid, capable of supporting shear-wave propagation.⁶⁻⁹ These studies provided an understanding of the physical processes by which sediment shear waves influence bottom reflection loss. Compressional-wave conversion at the substrate interface was established as the major mechanism generating shear waves in the sediment, and shear-wave propagation in the seafloor as the major acoustical mechanism affecting the long-range, low-frequency displacement field near the top of the substrate.¹⁰

While the influence of shear-wave excitation on low-frequency propagation was clearly demonstrated, unrealistically large values of shear-wave velocity were required in models to produce the expected levels of attenuation in shallow water environments.¹¹⁻¹³ One shear-wave related mecha-

nism potentially capable of increasing propagation loss at low frequencies was identified as a gradient driven coupling between shear and compressional waves. Since the strength of this coupling decreases with increasing frequency, its importance, if significant at all, will be mainly manifest at low frequencies. Vidmar and Foreman⁶ concluded that in deep-ocean sediments (clays and silts) the gradients of the geophysical parameters are so small as to render coupling effects negligible above about 3 Hz. However, for sand sediments, found primarily in shallow-water areas, in which near-surface gradients can be large,¹¹ the influence of coupling at low frequencies was uncertain.^{14,15} It was concluded that further experimental and theoretical work was required to better understand the bottom interaction process in naturally occurring sediments.

In similar studies Chapman also described methods for modeling bottom interaction at low frequencies and compared model results with loss data for various bottom environments.^{16,17} Other investigations of relevance have exploited the concept of "effective depth" to obtain an approximate description of normal mode propagation in various environments.^{18,19} The latest contribution based on this approach has incorporated energy loss into the reflection process.²⁰ All these studies have contributed to our understanding of the influence of the seabed on the acoustic field in the ocean, but all involve approximations of various sorts.

Our recent investigations of ULF (<1 Hz) and VLF (<10 Hz) seismoacoustic noise in the ocean²¹⁻²⁵ have led us also into a theoretical study of the reflection coefficient of complex seabed structures at very low frequencies. Because of the nature of the nonlinear wave-wave interaction source responsible for the main peak in the ULF noise spectrum, it has been necessary to examine the behavior of the reflection coefficient for both the homogeneous and inhomogeneous components of the wave-induced noise field. In these studies the influence of a layered bottom structure on reflection loss has been examined without invoking approximations except that the interfaces have been assumed to be smooth and parallel. The results of these studies have revealed aspects of the reflection process not previously recognized.

In these developments the bottom was first modeled as a number of homogeneous viscoelastic layers of different geoacoustical properties. (This approximation of the real environment was adopted as a sensible first step in the development of a more general depth-dependent model, but was also considered reasonable in view of the conclusions related to gradient-induced coupling at frequencies below 10 Hz, reached by Vidmar *et al.*^{6,14,15}) This paper provides a systematic presentation of these studies, and covers the behavior of the reflection coefficient with frequency and angle of incidence at the interface between a water-layer and a multilayered medium of increasing complexity. In a companion paper²⁶ we examine the behavior of the reflection coefficient when sediment porosity is introduced by way of the concepts inherent in the Biot–Stoll model.^{27–38}

In the interests of a more coherent presentation of the overall material the formalism for the general case, involving medium porosity, is developed in this first contribution. We start in Sec. I with a short introduction of the dispersion equations for a porous visco-elastic medium. In Sec. II we develop the numerical procedures required to calculate the reflection coefficient for this most general case, recognizing that the calculations for the simpler viscoelastic medium can then be made by neglecting the slow wave of the Biot model. Using this simplification the character of the reflection coefficient for a viscoelastic medium of varying complexity is examined in Sec. III. Both the frequency and wave-number domains are considered and the physical significance of the main features of the plots are discussed. A short summary is provided in Sec. IV.

I. THE DISPERSION EQUATIONS AND THE CONDITIONS GOVERNING BIOT WAVES IN POROUS MEDIA

As Stoll has provided comprehensive reviews of the extensive literature on the acoustics of porous media, only those contributions directly related to the development of this series of papers are referenced here. The reader is referred to Stoll's recent publications for a more detailed background.^{32–38}

According to Biot's theory,^{27–31,38} two kinds of dilatational and one type of shear wave can be propagated in a fluid-saturated, isotropic, porous-elastic medium. They satisfy, respectively, two dispersive equations. The first

$$\begin{pmatrix} \bar{H}l_c^2 - \omega^2\rho & \omega^2\rho_f - \bar{C}l_c^2 \\ \bar{C}l_c^2 - \omega^2\rho_f & m\omega^2 - \bar{M}l_c^2 - \frac{i \operatorname{sgn} \cdot \eta F \omega}{k_p} \end{pmatrix} = 0 \quad (1)$$

applies to the two dilatational waves and the other to the shear wave:

$$\begin{pmatrix} \mu l_s^2 - \omega^2\rho & \rho_f \omega^2 \\ -\omega^2\rho_f & m\omega^2 - \frac{i \operatorname{sgn} \cdot \eta F \omega}{k_p} \end{pmatrix} = 0. \quad (2)$$

In the above, η is the viscosity of the pore fluid, k_p the permeability of the sediment, and F is a complex function of the parameter $k_\eta \equiv a(\operatorname{sgn} \omega \rho_f / \eta)^{1/2}$, where a is the pore-size parameter; ρ is defined as a bulk density,

$\rho = \beta\rho_f + (1 - \beta)\rho_r$, in which ρ_f and ρ_r are the densities of the pore fluid and the skeletal frame, and β is the porosity; $m = \alpha\rho_f/\beta$, where α is a real constant. The symbol sgn represents the sign of the exponential term of the time factor $\exp(+i\omega t)$ or $\exp(-i\omega t)$. The other parameters \bar{H} , \bar{C} , \bar{M} , and μ are frequency-dependent porous elastic moduli of the medium, which are defined by Stoll,³⁸ while k and ω are here and later used to specify the horizontal wave number and the angular frequency, $\omega = 2\pi f$. Derivations of the basic equations governing wave propagation in unbounded porous media are given by Biot^{27–31} and Stoll.³⁸ In the literature dealing with this subject the symbols and definitions used are not consistent. To minimize confusion we will follow Stoll's conventions in this and related papers.

II. NUMERICAL PROCEDURE FOR THE CALCULATION OF REFLECTION COEFFICIENTS FOR A MULTILAYERED MEDIUM OF GENERAL PROPERTIES

We assume that a plane wave of unit amplitude $\Phi_{1\text{inc}} = e^{-i\gamma_1(z+H_1)+i(kx-\omega t)}$ is incident from water upon a seabed ($z = -H_1$) composed of parallel stratified layers of porous/visco-elastic layers overlying an elastic half-space. For convenience, however, all layers are modeled as porous. The redundant equations will be discarded by setting the amplitudes of the slow wave to zero in any layers that revert to a simple elastic form in the later analyses.

By defining the displacement vector of the solid frame and that of the pore fluid relative to the frame (in the n th layer) as

$$\mathbf{u}_n = \nabla\Phi_{ns} + \nabla \times \Psi_{ns}, \quad \mathbf{V}_n = \nabla\Phi_{nf} + \nabla \times \Psi_{nf} \quad (3)$$

where $\Psi_{ns} = (\mathbf{k}_0 \times \mathbf{n})\Psi_{ns}$ with \mathbf{k}_0 and \mathbf{n} being unit vectors in the direction of the horizontal wave-number vector (positive x direction in the present case) and the normal to the interfaces (positive z direction here). We can write the displacement components as

$$\begin{aligned} u_{nx} &= \frac{\partial\Phi_{ns}}{\partial x} + \frac{\partial\Psi_{ns}}{\partial z}, & u_{nz} &= \frac{\partial\Phi_{ns}}{\partial z} - \frac{\partial\Psi_{ns}}{\partial x}, \\ V_{nx} &= \frac{\partial\Phi_{nf}}{\partial x} + \frac{\partial\Psi_{nf}}{\partial z}, & V_{nz} &= \frac{\partial\Phi_{nf}}{\partial z} - \frac{\partial\Psi_{nf}}{\partial x}, \end{aligned} \quad (4)$$

and the stress and pressure components as

$$\begin{aligned} p_{nzz} &= \bar{H}_n \theta_n - 2\mu_n \frac{\partial u_{nx}}{\partial x} - \bar{C}_n \zeta_{pn}, \\ p_{nzx} &= \mu_n \left(\frac{\partial u_{nx}}{\partial z} + \frac{\partial u_{nz}}{\partial x} \right), & p_{fn} &= \bar{M}_n \zeta_{pn} - \bar{C}_n \theta_n. \end{aligned} \quad (5)$$

According to Stoll,³⁸ moduli \bar{H} , \bar{C} , and \bar{M} can be expressed through \bar{K}_b , the bulk modulus of the free-draining porous frame, K_f , the bulk modulus of the pore water and K_r , that of the solid frame as

$$\bar{H} = [(K_r - \bar{K}_b)^2 / (D - \bar{K}_b)] + \bar{K}_b + 4\mu/3, \quad (6)$$

$$\bar{C} = K_r(K_r - \bar{K}_b) / (D - \bar{K}_b), \quad (7)$$

$$\bar{M} = K_r^2 / (D - \bar{K}_b), \quad (8)$$

where

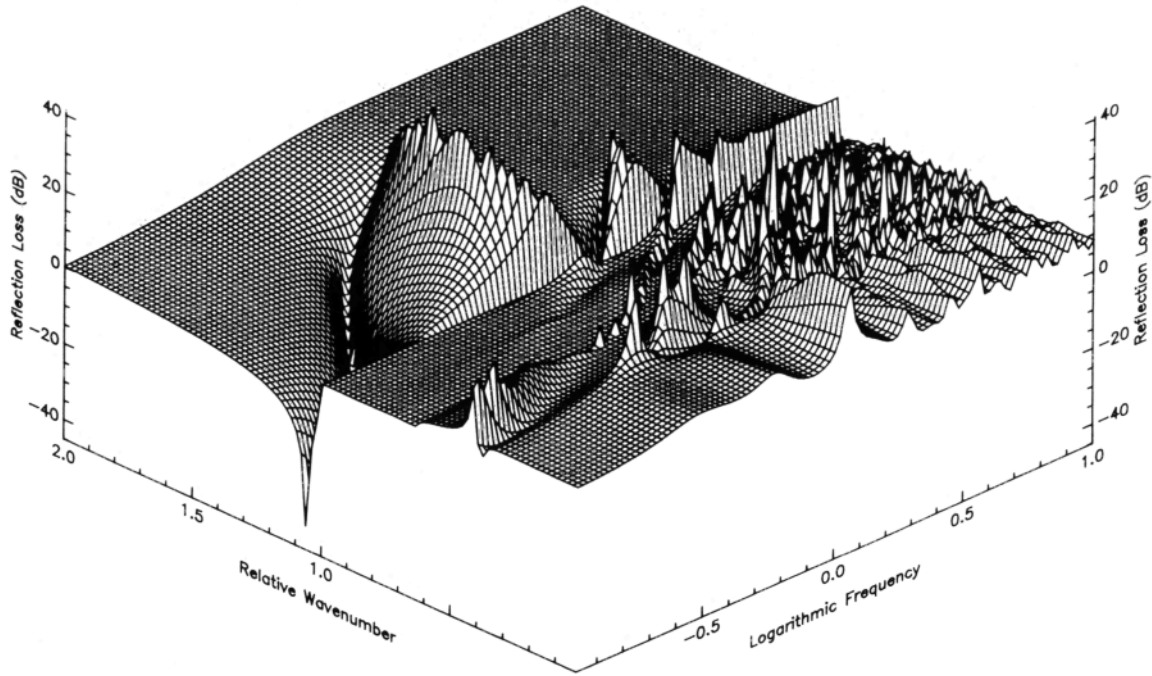


FIG. 1. Three-dimensional presentation of the reflection loss from a six-layered structure with the K-model parameters.

$$D = K_r [1 + \beta(K_r/K_f - 1)], \quad (9)$$

$$\zeta_{pn} = \nabla \cdot \beta_n (\mathbf{u}_n - \mathbf{U}_n) \equiv \nabla \cdot \mathbf{V}_n = \nabla^2 \Phi_{nf}, \quad (10)$$

$$\theta_n = \nabla \cdot \mathbf{u}_n = \nabla^2 \Phi_{ns}, \quad (11)$$

and β_n defines the porosity of the medium.

As was stated above, in the Biot/Stoll model three kinds of waves can propagate in a porous layer, the fast- and slow-compressional waves and the shear wave, with wave numbers l_{c1n} , l_{c2n} , and l_{sn} , respectively. Each of the three waves has a different amplitude depending on whether it is propagating in the solid frame or the pore water. The ratios of the two amplitudes for the three waves, defined as δ_{1n} , δ_{2n} , and δ_{3n} , are all functions of the medium constants,

$$\delta_{1n} = \frac{\bar{H}_n l_{c1n} - \omega^2 \rho_n}{\bar{C}_n l_{c1n} - \omega^2 \rho_{fn}}, \quad \delta_{2n} = \frac{\bar{H}_n l_{c2n} - \omega^2 \rho_n}{\bar{C}_n l_{c2n} - \omega^2 \rho_{fn}}, \quad (12)$$

$$\delta_{3n} = \frac{\rho_n}{\rho_{fn}} \left(1 - \frac{\mu_n l_{sn}^2}{\omega^2 \rho_n} \right).$$

Here, ρ_f is the density of the pore fluid, $\rho_n = \beta_n \rho_{fn} + (1 - \beta_n) \rho_{rn}$ with ρ_{rn} the density of the frame, all referred to the n th layer of the structure.

TABLE I. Sediment and substrate geoacoustic parameters.

| n | h_n | ρ_n (kg/m ³) | α_{nr} | β_{nr} | Q_{an} | Q_{bn} |
|-----|-------|-------------------------------|---------------|--------------|----------|----------|
| 1 | | 1540 | 1500 | | | |
| 2 | 325 | 2200 | 1560 | | 10 | |
| 3 | 850 | 2500 | 2000 | 1154 | 500 | 300 |
| 4 | 1650 | 2500 | 3100 | 1789 | 500 | 300 |
| 5 | 700 | 2500 | 3900 | 2251 | 500 | 300 |
| 6 | | 2500 | 4100 | 2367 | 500 | 300 |

The displacement potentials in each layer can be expressed as

$$\Phi_{ns} = \Phi_{ns1} + \Phi_{ns2},$$

$$\Phi_{nf} = \Phi_{nf1} + \Phi_{nf2} = \delta_{1n} \Phi_{ns1} + \delta_{2n} \Phi_{ns2}, \quad (13)$$

$$\Psi_{nf} = \delta_{3n} \Psi_{ns}$$

and

$$\left. \begin{aligned} \Phi_{ns1} &= A_{n1} e^{-i\gamma_{n1}(z+H_{n-1})} + B_{n1} e^{i\gamma_{n1}(z+H_n)} \\ \Phi_{ns2} &= A_{n2} e^{-i\gamma_{n2}(z+H_{n-1})} + B_{n2} e^{i\gamma_{n2}(z+H_n)} \\ \Psi_{ns} &= A_{n3} e^{-i\gamma_{n3}(z+H_{n-1})} + B_{n3} e^{i\gamma_{n3}(z+H_n)} \end{aligned} \right\} e^{ikx-i\omega t}, \quad (14)$$

where

$$\gamma_{n1} = \sqrt{l_{c1n}^2 - k^2}, \quad \gamma_{n2} = \sqrt{l_{c2n}^2 - k^2}, \quad \gamma_{n3} = \sqrt{l_{sn}^2 - k^2}.$$

Denoting the potential in the water column as

$$\Phi_1 = [e^{-i\gamma_1(z+H_1)} + R_b e^{i\gamma_1(z+H_1)}] e^{ikx-i\omega t}$$

with R_b defined as the reflection coefficient from the sea floor, the displacement vector and pressure field become

$$\mathbf{U}_1 = \nabla \Phi_1, \quad p_w = -\rho_1 \frac{\partial^2 \Phi_1}{\partial t^2}. \quad (15)$$

So, at $z = -H_1$,

$$\begin{aligned} U_{1z} &= -i\gamma_1(1 - R_b) e^{ikx-i\omega t}, \\ p_w &= \rho_1 \omega^2 (1 + R_b) e^{ikx-i\omega t}. \end{aligned} \quad (16)$$

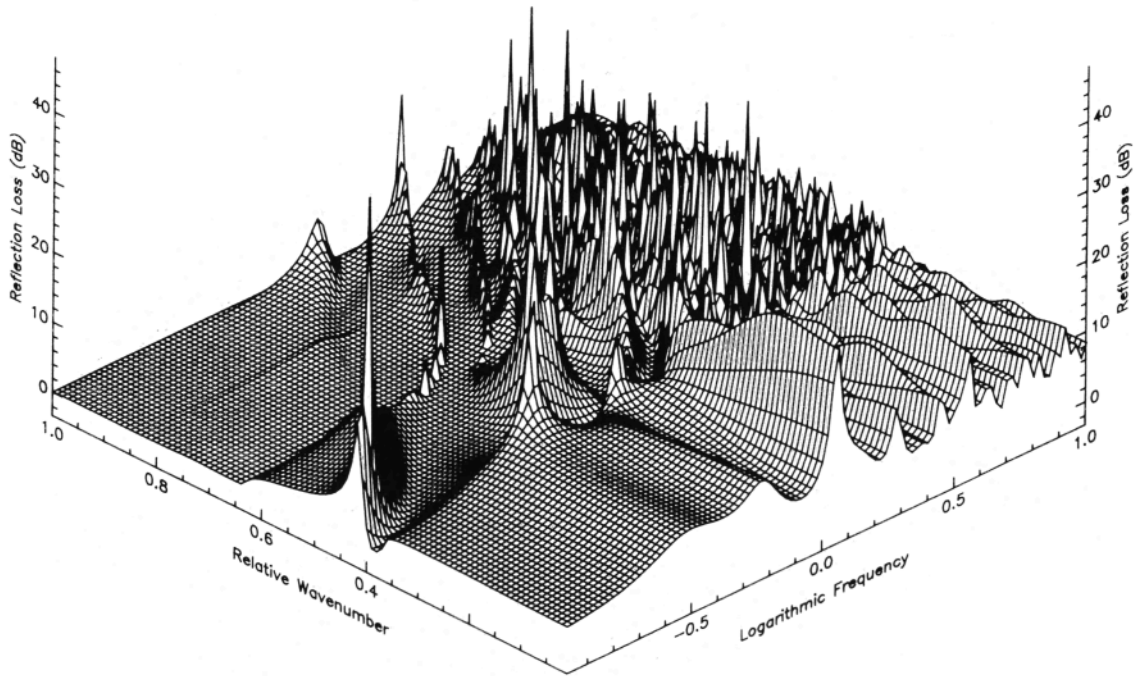


FIG. 2. The three-dimensional reflection loss over the homogeneous region of the presentation in Fig. 1.

The boundary conditions at the water–sediment interface, $z = -H_1$, require

$$U_{1z} = u_{2z} - V_{2z}, \quad -p_w = p_{2zz}, \quad (17)$$

$$0 = p_{2zx}, \quad p_w = p_{f2},$$

while at the interface of two porous layers, $z = -H_n$, the requirements are

$$u_{nz} = u_{n+1,z}, \quad u_{nx} = u_{n+1,x}, \quad (18)$$

$$u_{nz} - V_{nz} = u_{n+1,z} - V_{n+1,z},$$

$$P_{nzz} = P_{n+1,zz}, \quad P_{nzx} = P_{n+1,zx}, \quad P_{fn} = P_{f,n+1}.$$

For a N -layer model, there are $6 \times (N-1)$ parameters involved for the adjacent layers plus R_b and 3 amplitudes in the basement, altogether $6N-2$ unknowns, a number compatible with the number of equations.

In the case where one of the layers, say the $(n+1)$ th layer, is elastic, while both the n th and the $(n+2)$ th layers are porous, the boundary conditions at $z = -H_n$ become

$$u_{nz} = u_{n+1,z}, \quad u_{nx} = u_{n+1,x}, \quad (19)$$

$$u_{nz} - V_{nz} = u_{n+1,z}, \quad (\text{i.e., } V_{nz} = 0)$$

$$P_{nzz} = P_{n+1,zz}, \quad P_{nzx} = P_{n+1,zx},$$

and those at $z = -H_{n+1}$, become

$$u_{n+1,z} = u_{n+2,z}, \quad u_{n+1,x} = u_{n+2,x}, \quad (20)$$

$$u_{n+1,z} = u_{n+2,z} - V_{n+2,z}, \quad (\text{i.e., } V_{n+2,z} = 0)$$

$$P_{n+1,zz} = P_{n+2,zz}, \quad P_{n+1,zx} = P_{n+2,zx}.$$

Solving this system of algebraic equations numerically, we can establish the reflection coefficient and the amplitudes of the “up- and down-” going components of the three Biot waves in each layer. This analysis represents an extension of the numerical procedures for viscoelastic layers developed by Schmidt and Jensen.³⁹

III. THE FREQUENCY–WAVE-NUMBER SPECTRUM OF THE BOTTOM LOSS FOR A VISCOELASTIC MEDIUM

A. Preamble

In the remainder of this paper we examine the behavior of the bottom interaction for a multilayered viscoelastic medium. For ease of comparison with earlier studies the analysis to follow is presented in terms of bottom reflection loss. (In the treatment of the porous case, presented as a companion paper, it will be more appropriate to use the amplitude of the reflection coefficient.) An ocean bottom comprising six layers is considered. The codes developed for the present analysis have been tested against other published results.

B. Reflection loss for the K model

Figure 1 presents the reflection-loss of a six-layered geoacoustic structure which we designate as model K. Details of the structure, which is an approximate description of the environment in a recent New Zealand study,^{21,22} are listed in Table I. The parameters h_n , ρ_n , α_{nr} , β_{nr} , Q_{an} , and Q_{bn} are, respectively, the thickness, density, the real parts of the complex velocities, and the Q values of the compressional and shear waves of the n th layer.

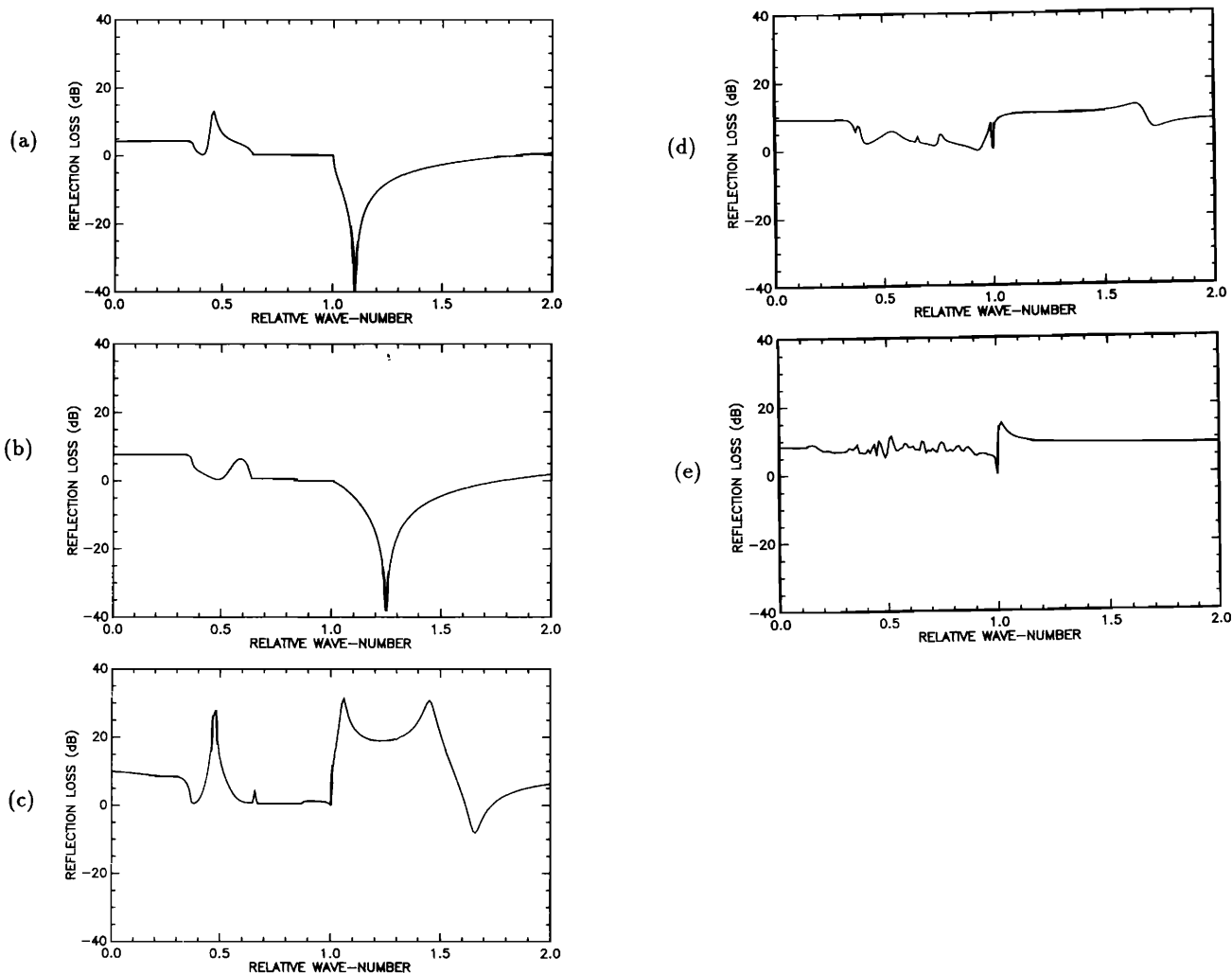


FIG. 3. Presentations of the wave-number dependence of the K-model reflection loss for the frequencies: (a) $f=0.147$ Hz, (b) $f=0.158$ Hz, (c) $f=0.63$ Hz, (d) $f=1.0$ Hz, and (e) $f=10.0$ Hz.

Figure 1 shows the general behavior of the reflection loss as a function of both the logarithmic frequency, $\log_{10}(f)$, over the range -1.0 to 1.0 (0.1 – 10 Hz), and the relative horizontal wave number, $u = k\alpha_1/\omega$, over the range 0.0 to 2.0 . Since u relates to the incident angle, θ , through $u = \sin \theta$, the range $0 \leq u \leq 1.0$ corresponds to a change in θ from 0 to $\pi/2$. In the above, α_1 is the sound velocity in seawater, $\omega = 2\pi f$, the angular frequency, and k the horizontal wave number. The right-hand side of the plot is thus simply a presentation of the usual angle-frequency dependence of loss. The left-hand side, on the other hand, shows that part of the inhomogeneous wave region for which $1.0 \leq u \leq 2.0$ (in the region $u > 2$ the reflection loss for the present model gradually tends to a constant value, as examined below, and the picture is flat and without structure). To show more clearly the structure in the homogeneous region (incident expanded angle 0° – 90°) this region is plotted in expanded form in Fig. 2.

In Fig. 3 selected cross sections at frequencies 0.147 , 0.158 , 0.63 , 1.0 , and 10.0 Hz are presented to show more clearly the character of the hidden section on the left-hand side of the three-dimensional (3-D) presentation. This set of plots demonstrates strikingly how much the character of the reflection loss can change with very small changes in frequency. For example, the peak of 30 dB near $u=0.5$ ($\theta=30^\circ$) at $f=0.63$ Hz disappears at $f=1.0$ Hz. Comparable variability with frequency occurs in the region $1.0 \leq u \leq 2.0$.

This variability emphasizes the care that must be exercised in interpreting the ordinary 2-D plots based on frequency or angular dependence. A 3-D presentation, on the other hand, offers some hope of identifying those truly significant features which reflect meaningful physical processes. In Fig. 1 such features are the regularly distributed “mountain chains” in the region $0.6 \leq u \leq 1.0$, the deep valley apparent at low frequencies around $u \geq 1.0$, and the high ridge and steep scarp located on the inhomogeneous side of the bound-

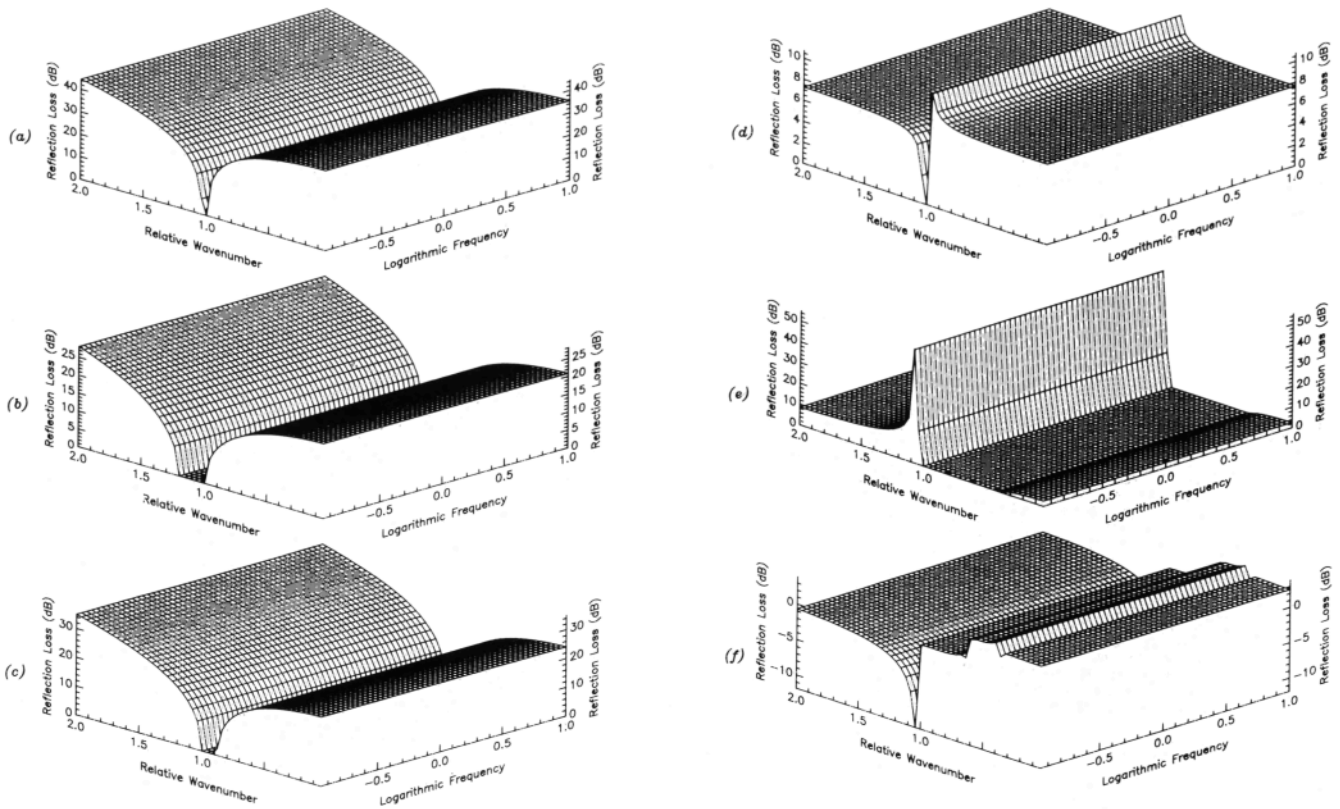


FIG. 4. Reflection-loss presentation from the interface between two semi-infinite media with the parameters $\rho_1 = \rho_2 = 1000 \text{ kg m}^{-3}$, $\alpha_1 = 1500 \text{ m s}^{-1}$, and $Q_{1a} = Q_{2a} = 10^8$ for the cases: (a) $\alpha_2 = 1450 \text{ m s}^{-1}$, (b) $\alpha_2 = 1250 \text{ m s}^{-1}$, (c) $\alpha_2 = 1700 \text{ m s}^{-1}$ and those with the parameters $\rho_1 = 1000$, $\rho_2 = 2500 \text{ kg m}^{-3}$, $\alpha_1 = 1500 \text{ m s}^{-1}$, and $Q_{1a} = 10^8$ for the cases: (d) $\alpha_2 = 1450 \text{ m s}^{-1}$, $Q_{2a} = 10^8$, (e) $\alpha_2 = 4100 \text{ m s}^{-1}$, $Q_{2a} = 10^8$, (f) $\alpha_2 = 4100$, $\beta_2 = 2367 \text{ m s}^{-1}$, $Q_{2a} = 500$, $Q_{2b} = 300$.

ary at $u=1.0$. These interesting features are examined in detail in the following sections.

C. The case of two contacting half-spaces

We begin by considering the simplest possible model, comprising a water layer and a second layer that can be either a liquid or a solid half-space.

Figure 4 presents the 3-D reflection loss for two liquid layers with slightly different parameters as indicated in the figure caption. As expected these plots show no frequency dependence in the reflection loss. For this simple model the

reflection coefficient, R_b , takes the well known form

$$R_b = \frac{m\sqrt{1-u^2} - \sqrt{n^2-u^2}}{m\sqrt{1-u^2} + \sqrt{n^2-u^2}}, \quad (21)$$

where $m = \rho_2/\rho_1$, $n = \alpha_1/\alpha_2$. The loss, $LR_b = -20\log_{10}|R_b|$, will assume different values in different cases.

Here and in the companion paper²⁶ attenuation is included through the imaginary part of the complex velocities $\alpha_1, \alpha_2, \beta_2$, etc. For the ideal case when attenuation is ignored, the values of the reflection loss can be summarized as follows:

$n > 1$ [see Fig. 4(a), (b), and (d)]

$$\begin{array}{ll} 0 \leq u < 1 & LR_b > 0 \\ 1 \leq u < n & LR_b = 0 \quad (R_b = 1) \\ n < u & LR_b > 0 \\ u \rightarrow \infty & LR_b \rightarrow -20 \log_{10}[(m-1)/(m+1)] \\ u \rightarrow 0 & LR_b \rightarrow -20 \log_{10}[(m-n)/(m+n)] \end{array}$$

$n < 1$ [see Fig. 4(c) and (e)]

$$\begin{array}{ll} 0 \leq u < n & LR_b > 0 \\ n \leq u < 1 & LR_b = 0 \\ u > 1 & LR_b > 0 \end{array}$$

If $\rho_2 = \rho_1$, as is the case in Fig. 4(a) and (b), the loss becomes infinite when $u \rightarrow \infty$, but when $\rho_2 \neq \rho_1$ remains bounded for $u \rightarrow 0$ or ∞ . As an example we can consider version (d) of the model, for which $m = 2.5$ and $n = 1.035$. In this case the limit

$$R_b = \frac{m \sqrt{1-u^2} [4u^2 \sqrt{n_a^2 - u^2} \sqrt{n_b^2 - u^2} + (n_b^2 - u^2)^2] - n_b^4 \sqrt{n_a^2 - u^2}}{m \sqrt{1-u^2} [4u^2 \sqrt{n_a^2 - u^2} \sqrt{n_b^2 - u^2} + (n_b^2 - 2u^2)^2] + n_b^4 \sqrt{n_a^2 - u^2}}, \quad (22)$$

where $n_a = \alpha_1 / \alpha_2$ and $n_b = \alpha_1 / \beta_2$. Again in the ideal case, it can be seen that when $u = n_a = 0.366$ and $u = n_b = 0.634$ ($\alpha_2 = 4100 \text{ m s}^{-1}$, $\beta_2 = 2367 \text{ m s}^{-1}$), $|R_b| = 1$ and $LR_b = 0$. In Fig. 4(f), this zero point is not very well defined because finite values have been assigned to Q_{2a} and Q_{2b} .

Other important features apparent in Fig. 4(f) are the deep valley immediately beyond $u = 1.0$ and the ridge between $n_a \leq u < n_b$. In the valley LR_b is less than zero, which means R_b is much greater than one. The significance of R_b exceeding unity calls for comment, since this value seems to violate the laws of energy conservation. Understanding follows from an examination of the physical processes involved.

To establish a wave field the source must supply energy. In the steady state a balance is established between the source and the field. In the case of homogeneous waves ($u \leq 1$), energy flows in the propagation direction of the incident and reflected wavefront. From the standpoint of an observer on the source side of an interface, some energy passes through the boundary and some is reflected. Since there is no source on the underside of the boundary energy conservation requires that the reflected energy cannot exceed that incident, which means that $R_b \leq 1$. In the inhomogeneous case however, energy flows parallel to the interface. As Frisk⁴⁰ has pointed out, it is not possible in this situation to resolve the incident and reflected energy, as both components flow in the same direction. All that can be identified is the energy flow along both sides of the boundary. If we therefore retain the definition of R_b , it follows that $|1 + R_b|$ will be proportional to the confined energy.

At the value of u at which the Scholte interface wave is excited (say for $u = 1/0.998$ when $\alpha_2 = \sqrt{3} \beta_2$), more energy is drawn from the source to establish the new balance. When balance (steady state) is established the amplitude of the interface-wave can become very high so that $R_b \gg 1$ and $LR_b \rightarrow -\infty$. It is this situation that accounts for the deep valley apparent in Fig. 4(f) at around $u \geq 1$.

The ridge in the homogeneous region is simply a manifestation of the feature always observed in the two-dimensional presentation of reflection-loss versus angle. It represents the energy loss between the two critical angles, θ_s and θ_p for the substrate,⁷ and is attributed to the increased conversion of compressional to shear wave propagation in the basement. A plausible explanation for this is that within this range of angles the direction of the particle motion of the reflected compressional wave is very close to that of the shear wave in the basement. In fact from Fig. 5(a) we see

value of LR_b is 7.36 as $u \rightarrow \infty$, and 7.65 as $u \rightarrow 0$, values which agree with those shown in Fig. 4(d). The results for a water layer overlying a solid half-space are presented in Fig. 4(f). In this situation the general expression for R_b is:

that angle of incidence θ_{p1} and the angle of transmitted shear-wave θ_{s2} , are related by

$$\sin \theta_{s2} = \sqrt{n_b^2 - \sin^2 \theta_{p1}}.$$

An examination of the difference between θ_{s2} and θ_{p1} , $\Delta \theta_{ps}$, as a function of $u/n_b (= k \beta_2 / \omega)$ is shown in Fig. 5(b) for the ideal case of $\alpha_2 = 4100$ and $\beta_2 = 2367 \text{ m s}^{-1}$. When $u/n_b \sim 0.844$ ($\theta_{p1} = 32.35^\circ$, $\Delta \theta_{ps} = 0$), the directions of particle motion in both the reflected (compressional) and transmitted (shear) waves are parallel. At the lower end of this range where the value $u/n_b = \beta_2 / \alpha_2 = 0.577$, the compressional wave is totally reflected.

Another striking feature of this set of plots is the steep scarp seen clearly in Fig. 4(e). It is not difficult to show that

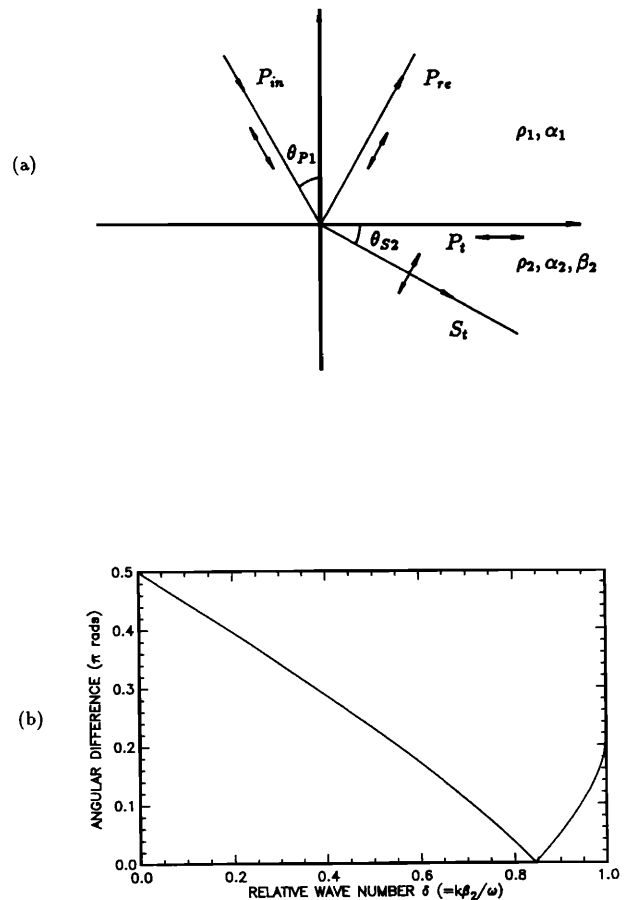


FIG. 5. Presentations of (a) the wave coupling at a liquid–solid interface and (b) the angular difference between the reflected compressional and the transmitted shear wave.

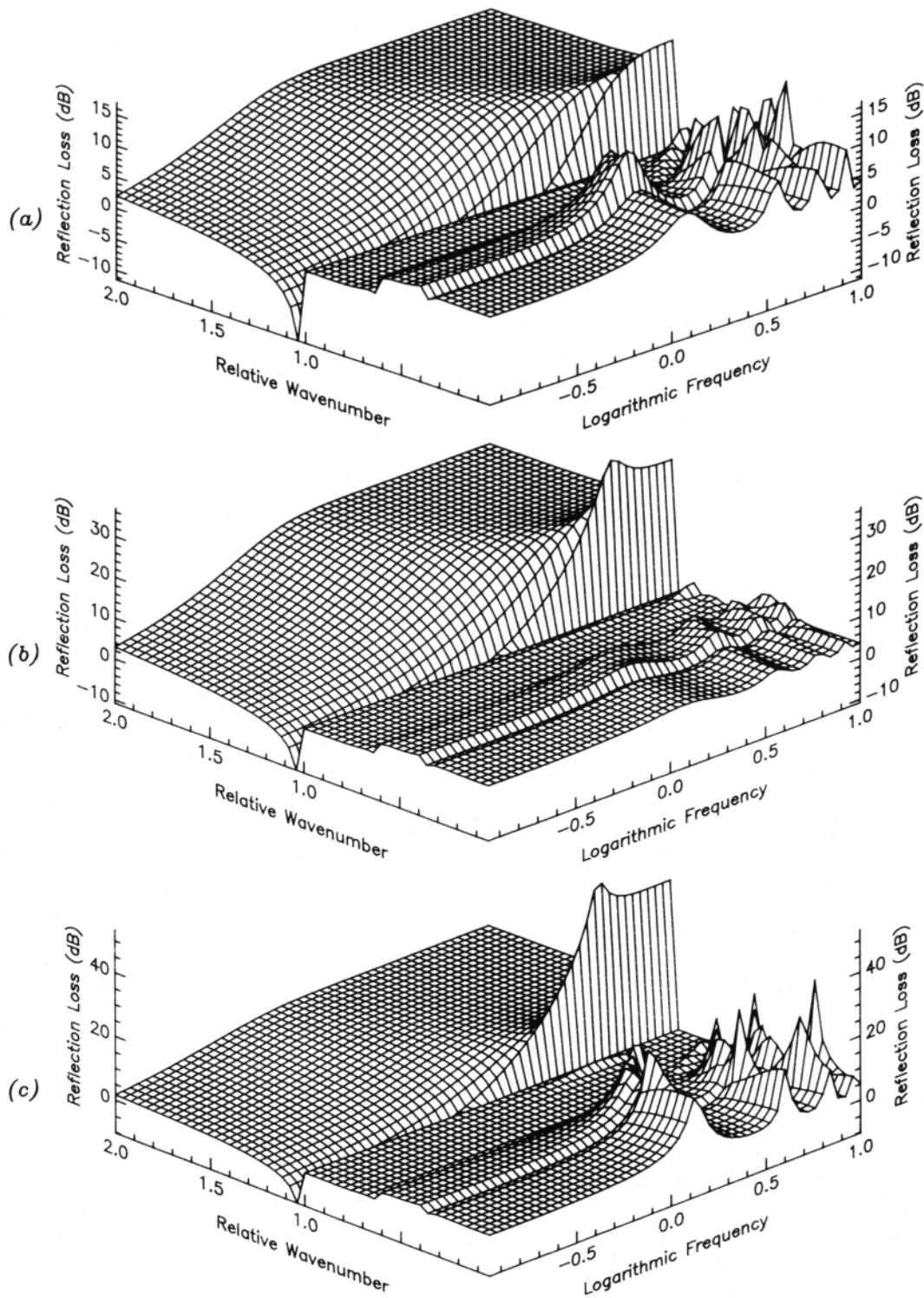


FIG. 6. Reflection loss from a three-layered structure with a middle layer consisting of (a) silt, (b) clay, and (c) sand.

this sharp increase in the reflection loss corresponds to the onset of total transmission. From Eq. (21) it can be seen that when u takes the value $\sqrt{(m^2 - n^2)/(m^2 - 1)}$, about 1.08, R_b becomes zero and thus LR_b tends to infinity. The same happens in the case of Fig. 4(d) where the total transmission appears at $u=0.993$.

D. The three-layer model

1. Where the middle layer is a low rigidity sediment

We now increase the complexity of the model by inserting a sediment with low rigidity and modest attenuation in between the water layer and the solid basement. The

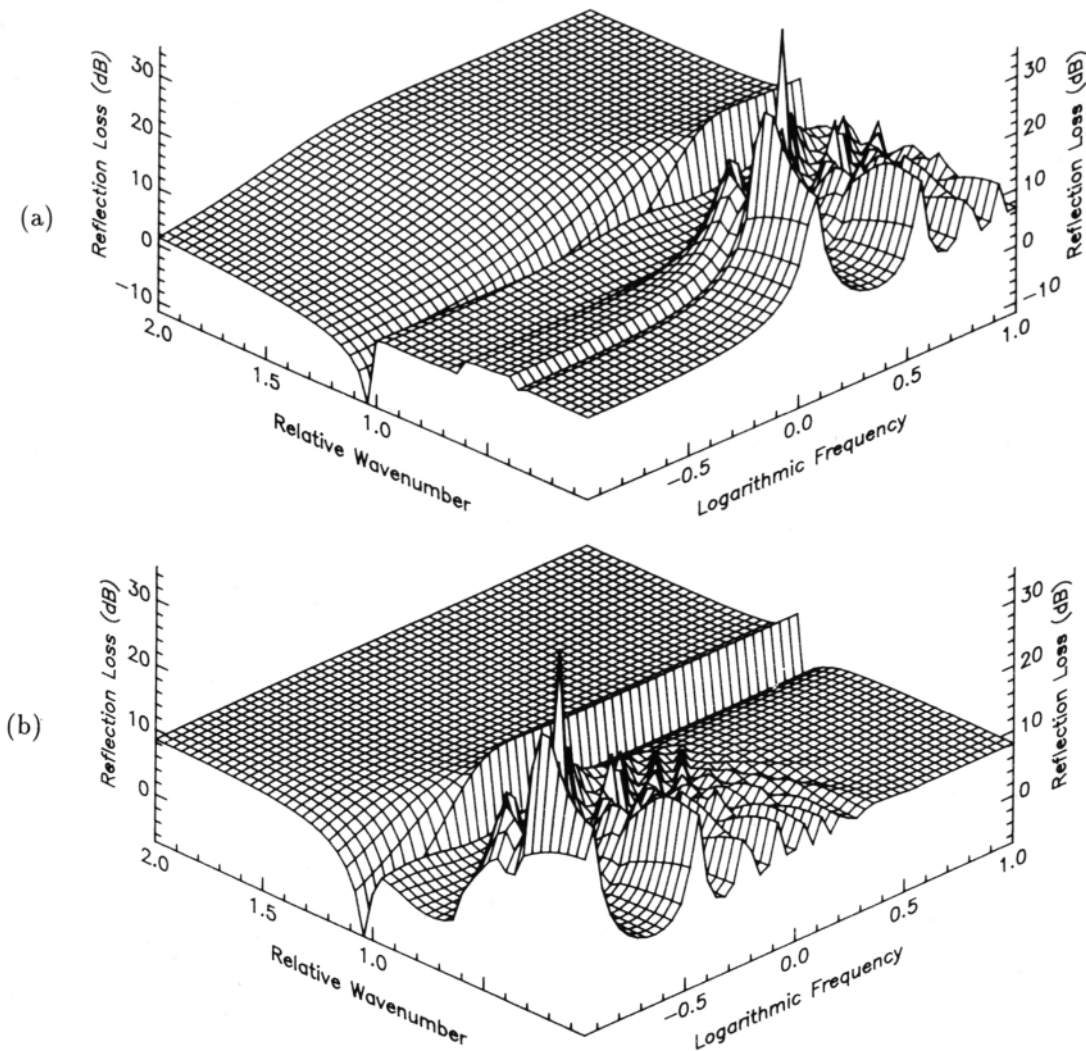


FIG. 7. Reflection loss from a three-layered structure with a middle layer consisting of (a) Maui sediment of thickness 325 m and (b) Maui sediment of thickness 3250 m.

reflection-loss plots for four different sedimentary materials are presented; in Fig. 6— for (a) silt; (b) clay; (c) sand; and in Fig. 7(a) a material characteristic of the Maui region and described by Kibblewhite.²² In each case the middle layer is 325 m thick. Values of the relevant parameters are listed in Table I for Fig. 7(a) and in Table II for Fig. 6(a)–(c).

Comparison with Fig. 4(f), the case without the middle sedimentary layer, shows that two new characteristics have developed. The first is an apparently periodic structure at high frequencies, which contrasts with the unchanged picture at low frequencies. The second is the steep scarp at high

frequencies in the inhomogeneous region of the plot. Both features can be explained satisfactorily by a comparison with previous examples.

The periodic structure develops as the result of interference between the incident and reflected wave energy associated with the middle layer. Reflection loss peaks are expected when

$$\sqrt{1-u_n^2} f_n = [\frac{1}{2}(n+1) - \phi/(2\pi)](\alpha_2/h),$$

where ϕ is the sum of the phase changes produced by reflection at the upper and lower boundaries of the middle layer. As a rough estimate of the peak frequencies involved we can set $\phi=0$ and $u_n=0$ (normal incidence), which leads to $\log_{10}(f_0)=0.37$, $\log_{10}(f_1)=0.675$, $\log_{10}(f_2)=0.85$, and $\log_{10}(f_4)=0.976$, values which coincide closely with the peaks of the structure apparent in Figs. 6 and 7(a). Furthermore the increase in f_n with relative wave number u_n , predicted by the above formula, is also confirmed by the trends of the peaks in Figs. 6 and 7(a).

TABLE II. Sediment and substrate geoaoustic parameters.

| | α | β | ρ | Q_a | Q_b |
|----------|----------|---------|--------|-------|-------|
| Water | 1540 | | 1000 | | |
| Clay | 1550 | | 1270 | 150 | |
| Silt | 1538 | | 1700 | 120 | |
| Sand | 1753 | | 2050 | 320 | |
| Basement | 5700 | 2700 | 2600 | 2000 | 250 |

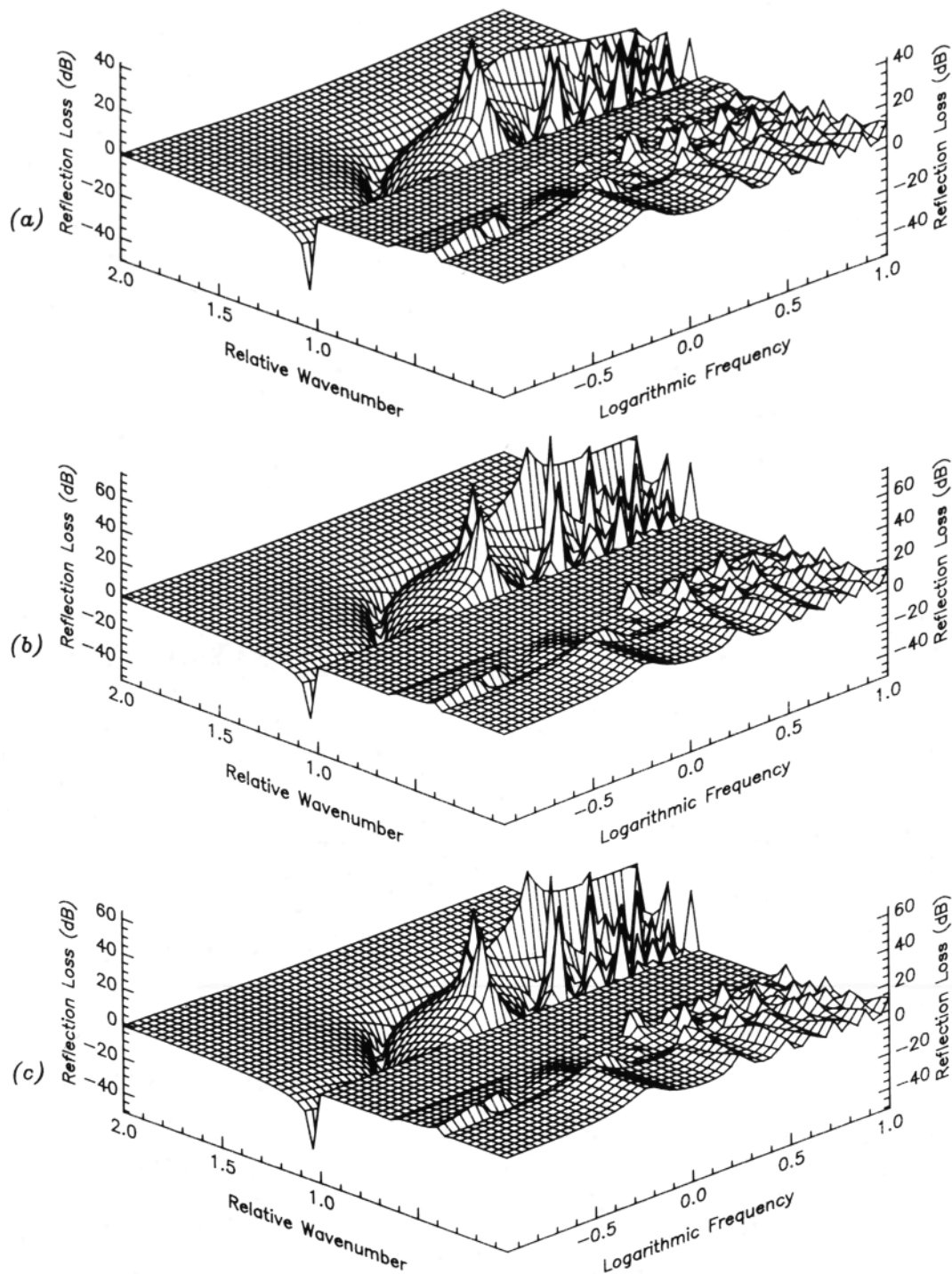


FIG. 8. Reflection loss from a three-layered structure in which the solid middle layer has the properties $\alpha_2=2000$, $\beta_2=1154 \text{ m s}^{-1}$ for the cases: (a) $Q_{2a}=Q_{3a}=500$, $Q_{2b}=Q_{3b}=300$; (b) $Q_{2a}=Q_{3a}=Q_{2b}=Q_{3b}=10^8$; (c) $Q_{2a}=Q_{2b}=10^8$, $Q_{3a}=Q_{3b}=500$.

The behavior in the inhomogeneous region appears to reflect a mixture of the effects apparent in the two-layer model—see Fig. 4(e) and (f). For instance, at low frequencies the situation in Figs. 6 and 7(a) has changed little from that depicted in Fig. 4(f). This is to be expected given that the wavelength at these frequencies is much greater than the thickness of the middle layer of the three-layer model. At these frequencies the inhomogeneous wave decays little from

the top to the bottom of the layer, which can thus be regarded as thin and transparent to these frequencies. The reflection-loss structure at low frequencies is not therefore expected to differ significantly from that of the simpler model in which the sedimentary layer is absent—see Fig. 4(f). At high frequencies on the other hand, the thickness of the layer (325 m) is equivalent to nearly two wavelengths, so that the lower boundary is outside the effective range of influence of the

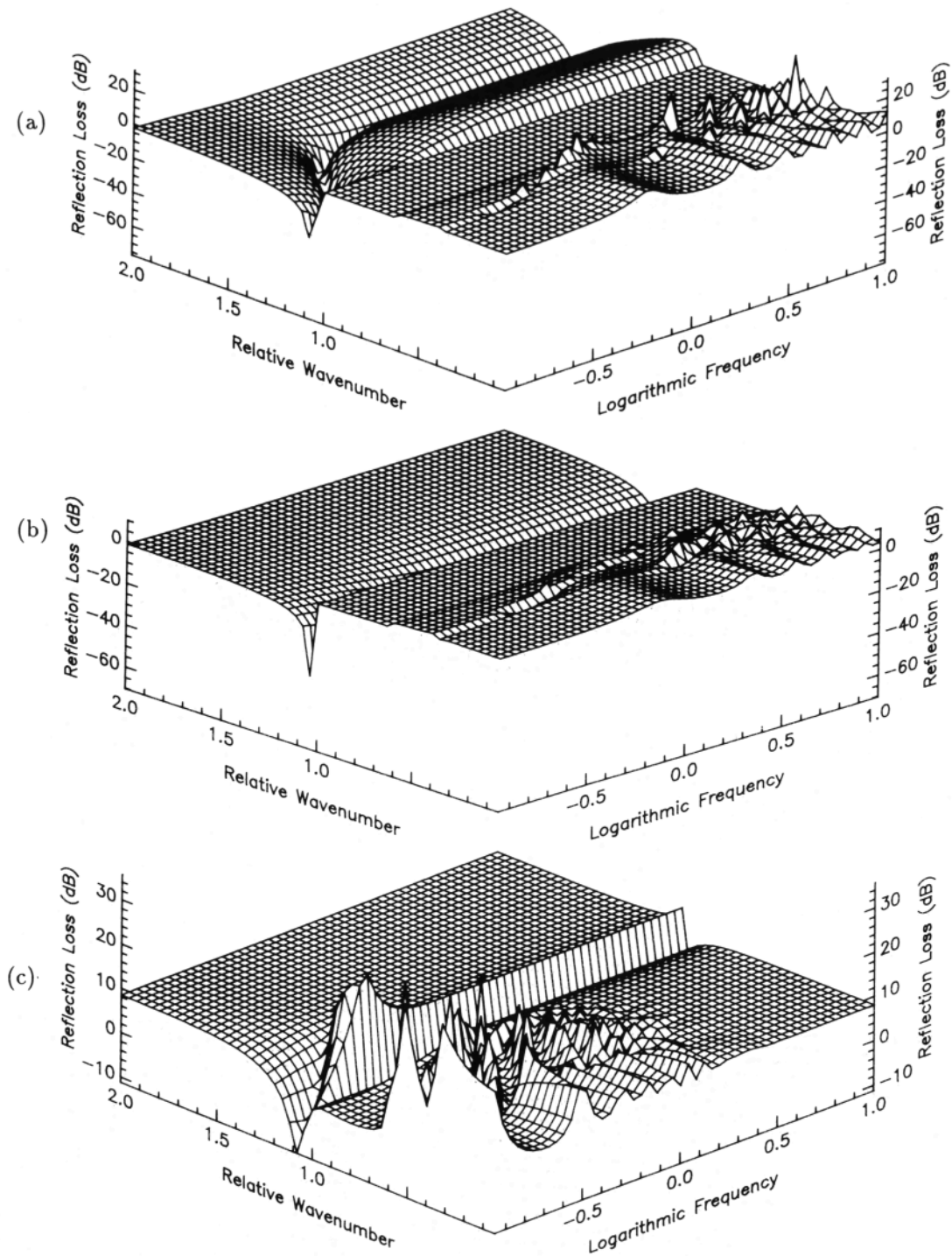


FIG. 9. Reflection loss from a three-layer structure with a solid middle layer having the properties $Q_{2a}=Q_{3a}=Q_{2b}=Q_{3b}=10^8$ for the cases: (a) $\alpha_2=2000$, $\beta_2=1800 \text{ m s}^{-1}$, (b) $\alpha_2=2500$, $\beta_2=2000 \text{ m s}^{-1}$, (c) $h_2=3250 \text{ m}$, $\alpha_2=2000$, $\beta_2=1154 \text{ m s}^{-1}$.

inhomogeneous field generated at the upper boundary. The layer is thus physically thick and impenetrable at those frequencies, and at about $u=1.01 R_b$ tends to zero and LR_b to very high values. Figure 7(b) presents the extreme situation when the thickness of the middle layer is increased by a factor of 10. It clearly shows that in the high-frequency region the overall behavior of the reflection loss is character-

istic of the model involving the two liquid layers; i.e., the solid basement is now effectively located below the "hidden-depth,"⁴¹ and the environment is adequately described by a model involving only two liquid layers.

A transition region between these two extremes completes the picture and all the characteristics of Figs. 6 and 7(a) are accounted for.

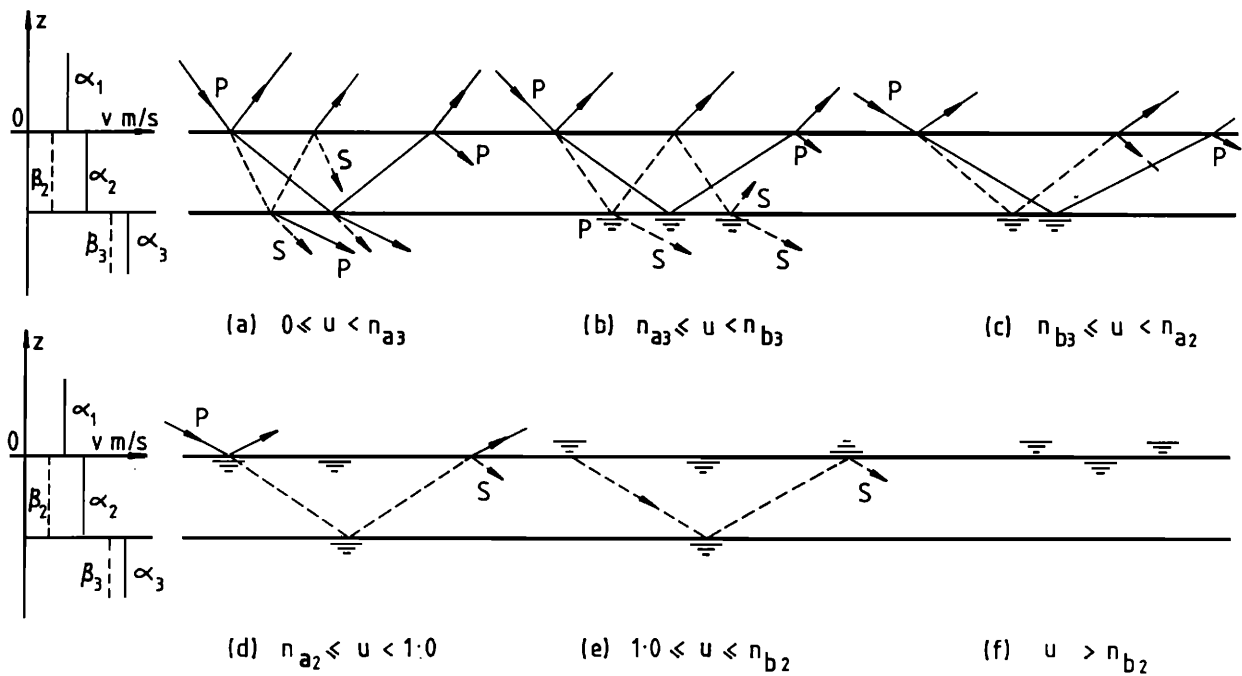


FIG. 10. Ray path representation of the reflection from various bottom structures with a low shear-wave velocity layer in between the water and solid basement half-spaces.

2. Where the middle layer is a solid sediment

We now change the middle layer of the three-layer model from a liquid to a solid, and assume in the first instance that the shear-wave velocity in the layer is less than both the sound velocity in water and in the basement. The reflection-loss contours in the inhomogeneous region are now seen to be changed significantly—see Figs. 8(a)–(c) and 9(a). In all these cases the basement is considered to be that of the K model, the parameters for which are listed in Table I.

Figure 8(a) depicts the situation when the shear-wave velocity of the middle layer is less than the velocities in the adjacent layers (a particular property of the K model), while Figs. 8(b)–(c) and 9(a) and (b) indicate the consequences of modifying the parameters of the middle layer.

From a comparison with Fig. 6(a) it is apparent that in Fig. 8(a) and (b) some additional structure has developed at high frequencies in the inhomogeneous region near $u=1$. Further, in the homogeneous region the periodic structure so obvious in Fig. 6(a) persists in Figs. 8 and 9(a) but is less pronounced.

The development of the structure in the inhomogeneous region can be explained in terms of mode effects in the “low-velocity” middle layer. The general situation in respect of one such model is depicted in Fig. 10(e). Because the shear-wave velocity β_2 is assumed to be less than the sound velocity in water, α_1 , and those in the basement, α_3 , and β_3 , the eigenray will experience total reflection at both the upper and lower boundaries. In the interest of simplicity we approximate this layer as a perfect waveguide with velocity β_2 . Each mode should then satisfy the eigenequation $\gamma_n h = \pi n$, where

$$\gamma_n = (\omega/\alpha_1) \sqrt{n_{b2}^2 - u_n^2} = (\omega/\alpha_1) \sin \theta_n \quad \text{and} \quad n_{b2} = \alpha_1/\beta_2.$$

It follows that

$$f_n = \frac{n\alpha_1}{2\sqrt{n_{b2}^2 - u_n^2}h} = \frac{n\alpha_1}{2h \sin \theta_n} \quad (23)$$

or

$$u_n = \sqrt{n_{b2}^2 - \frac{n^2 \alpha_1^2}{4h^2 f_n^2}}. \quad (24)$$

It is now appropriate to consider three distinct regions.

In the region $0 \leq u < \alpha_1/\alpha_3 = 0.366$ [Fig. 10(a)] some of the energy incident on the layer will penetrate to the basement and some will suffer partial reflection. Of this energy some will return to the water and some remain within the layer. [In an elastic medium a train of either compressional(P) or shear(S) wave incident upon the boundary generates both a reflected shear and compressional wave, P-S and P-P, or S-S and S-P. To keep the figures simple, however, we have deliberately drawn only the S-S or P-P components.] Interference between the incident and reflected energy within the layer then leads to “leaking modes” (mainly compressional) being established in the layer and accounts for the periodic structure evident in the plots at low relative wave numbers. At larger values of u , where $\alpha_1/\alpha_3 < u < \alpha_1/\beta_3$ [Fig. 10(b)], the compressional-wave component within the layer will be “totally” reflected by the lower boundary (part of the compressional-wave energy converts to shear waves that penetrate into the basement). In this region the shear-wave component can still penetrate to the basement, but when $\alpha_1/\beta_3 < u \leq 1$ [Fig. 10(c) and (d)] both the compressional

and shear-wave components are totally reflected by the lower boundary. However since the layer has been attributed with a lower attenuation than the sediment layer discussed in Figs. 6 and 7, less energy is absorbed (by leaking modes) and the periodic structure in the reflection loss is much less pronounced.

Finally, when u is such that $1 \leq u < n_{b2} (=1.3)$ [Fig. 10(e)], only modes of the shear-wave component can be excited within the layer, generation of the ordinary compressional-wave modes now being absent by virtue of the fact that $\alpha_2 > \alpha_1$. This shear-wave energy is now constrained as “trapped modes” (rather than leaking modes), since total reflection occurs at both boundaries of the layer. This leads to a high reflection loss as this energy is now not leaking back to the water.

In addition to the effects described above another resonance mechanism can occur. This involves the excitation of an interface wave on the lower boundary of the layer. At low frequencies the inhomogeneous wave can still have sufficient amplitude at the depth of the lower boundary to excite an interface wave in this boundary. At high frequencies on the other hand this cannot occur and the mode effects become dominant. This selective behavior is demonstrated clearly in the reflection loss plots of Figs. 8 and 9. The deep valley associated with the interface wave at low frequencies gradually disappears to be replaced at high frequencies by the periodic structure associated with mode behavior.

It is apparent from Eqs. (23) and (24) that the position of the first peak in this structure is a function of both frequency and relative wave number:

$$f_1 = \frac{\alpha_1}{2h_2 \sqrt{n_{b2}^2 - u_1^2}} \quad (25)$$

The increase in f_1 with u_1 predicted in Eq. (25) accounts for the curved form of the structure at the high-frequency end of the inhomogeneous region. Moreover the maximum value of Eq. (5) occurs when u_1 equals the imaginary part of n_{b2} , approximately 1.3 in this case. Beyond this value the contours again become flat as is shown in Fig. 8(a). This behavior can also be seen in Figs. 11 and 12. Figure 11(a) and (b) shows the dependence of reflection loss on wave number at frequencies of 1.0 and 7.94 Hz, while Fig. 12(a)–(e) shows the frequency dependence at $u = 0.1, 0.3, 1.1, 1.3,$ and 1.5 . We see that when u increases to 1.1 [Fig. 12(c)] the level of RL increases dramatically and is characterized by multiple peaks. With a further increase in u to 1.3 only a single peak remains [Fig. 12(d)] and this too disappears when $u = 1.5$ [Fig. 12(e)].

Returning now to Figs. 8 and 9 we can assess the relative importance of absorption, and the influence of the shear-wave speed. From Fig. 8(a) and (c) we observe that a decrease in the attenuation of the layer produces a greater level change in reflection than a comparable change in the basement attenuation—see Fig. 8(b) and (c).

The critical influence of the shear-wave velocity of the middle layer is demonstrated in Figs. 8(c)–9(b). When the shear-wave velocity is increased from 1154 to 1800 m s^{-1} , which exceeds the sound velocity in water, much of the structure in the inhomogeneous region disappears—see Fig.

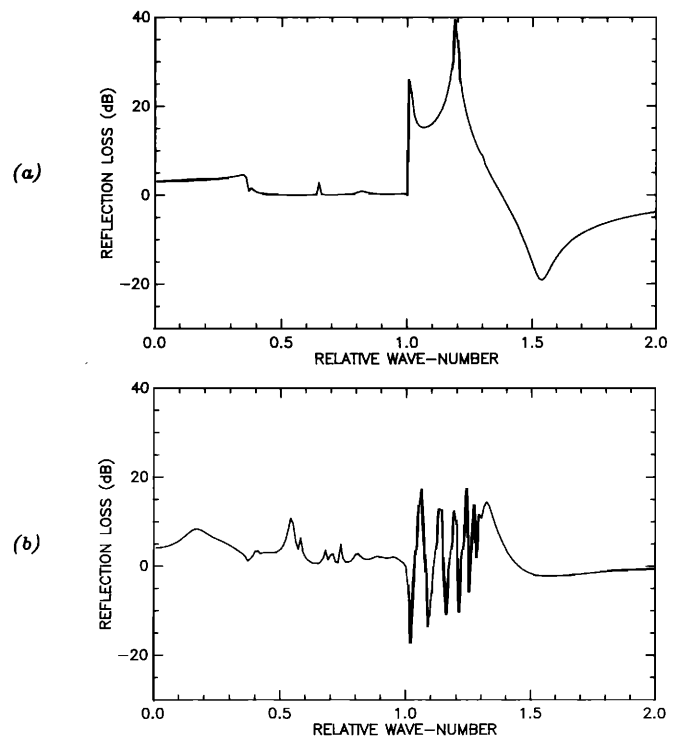


FIG. 11. Wave-number dependence of the reflection loss for the selected cases of constant frequency (a) $f=1.0$ Hz, $\log_{10} f=0$ and (b) $f=7.94$ Hz, $\log_{10} f=0.9$.

9(a). This comes about in the following way. As noted earlier the decay of the inhomogeneous wave means that the middle layer is effectively opaque to high frequencies. At low frequencies on the other hand, energy can penetrate the layer to excite an interface wave at the lower boundary and this results in the second valley and peaky structure evident in Fig. 8(c). The frequency and wave-number dependence of the critical depth for interface wave excitation produces the curved transition region between the two extremes of frequency.

The precise nature of this frequency dependence is influenced by the wave velocity in the layer. An increase in wave velocity can render the middle layer transparent over much of the frequency range considered here. The valley associated with the interface wave at the upper boundary showed that, in the inhomogeneous region, this wave becomes relatively less significant and disappears along with the structure at high frequencies leaving only the valley associated with the interface wave at the lower boundary. The development of these effects is demonstrated in Fig. 9(a) and (b), in which the shear velocity is 1800 and 2000 m s^{-1} , respectively. Figure 9(c) again shows the situation when the thickness of the middle layer is increased by ten times. These presentations show that if the velocities in a multilayered structure increase with depth from layer to layer, so that no “low” velocity layer is present in the model, the reflection loss in the inhomogeneous region will be relatively flat and featureless.

E. The influence of additional solid layers

We are now in a position to consider the implications of the complete six-layer K model. Figure 13 shows the effect

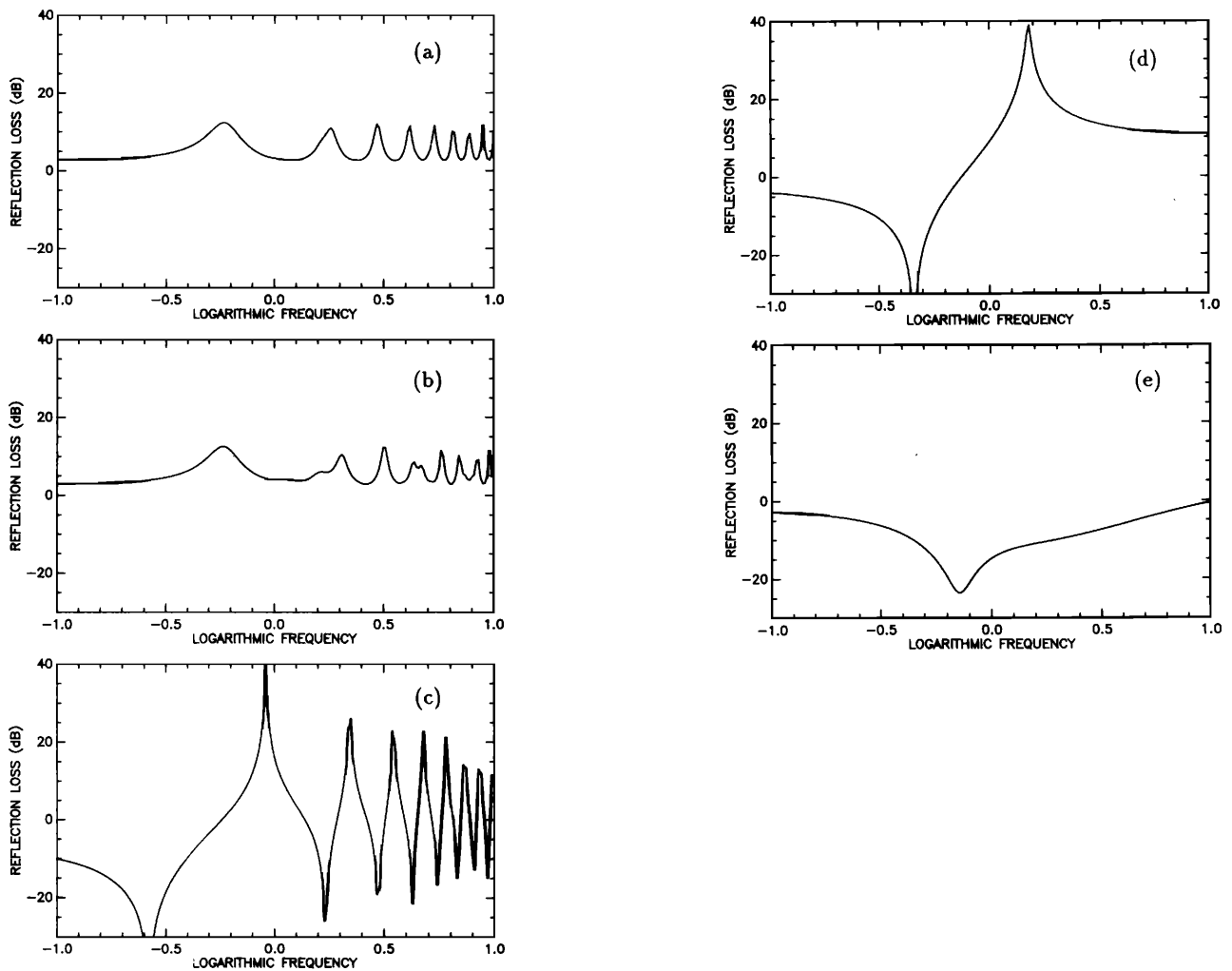


FIG. 12. Frequency dependence of the reflection loss for the selected cases of constant wave number: (a) $u=0.1$, (b) $u=0.3$, (c) $u=1.1$, (d) $u=1.3$, and (e) $u=1.5$.

of adding sequentially the second, fourth, and fifth layers of the model to the simplified model considered above, which consists of only the water column, the third layer, and the basement. The reflection-loss structure clearly changes little with the addition of each of the deeper layers. This suggests that, apart from the water and basement, the unconsolidated sedimentary layer and the solid sublayer characterized by the relatively slow shear-wave velocity, have the greatest influence on the reflection loss. The addition of further layers adds more detail but does not influence the basic nature of the frequency-wave-number dependence of the reflection loss to any marked degree.

IV. SUMMARY

In this contribution we have examined the basic procedures involved in calculating the plane-wave reflection loss from a viscoelastic multilayered medium of general properties. The reflection-loss behavior of a viscoelastic structure as a function of both frequency and wave number has been discussed, and both the homogeneous and inhomogeneous

regions have been explored. The three-dimensional presentation used and the inclusion of the inhomogeneous region have emphasized the limitations of a simple two-dimensional analysis and warned of the danger of drawing conclusions on reflection-loss behavior on the basis of a few samples at individual frequencies or grazing angles.

The results have also identified several major characteristics of the behavior of the reflection loss in a multilayered bottom. It is shown that the reflection loss is controlled largely by the properties of the unconsolidated sediment layer, the basement and any sublayer with relatively low shear-wave speed (if it exists). Periodic structure occurring at high grazing angles is shown to result from "hybrid modes" formed in the sediment layer, while at low grazing angles ($u \leq 1$) and in the inhomogeneous region ($u > 1$) such structure is found to result from trapped modes excited in a solid sublayer characterized by a relatively low shear-wave speed. The excitation of an interface wave at the lower interface of such a sublayer can lead to a deep valley ($R_b \gg 1$) in the inhomogeneous region at low frequencies. As the frequency

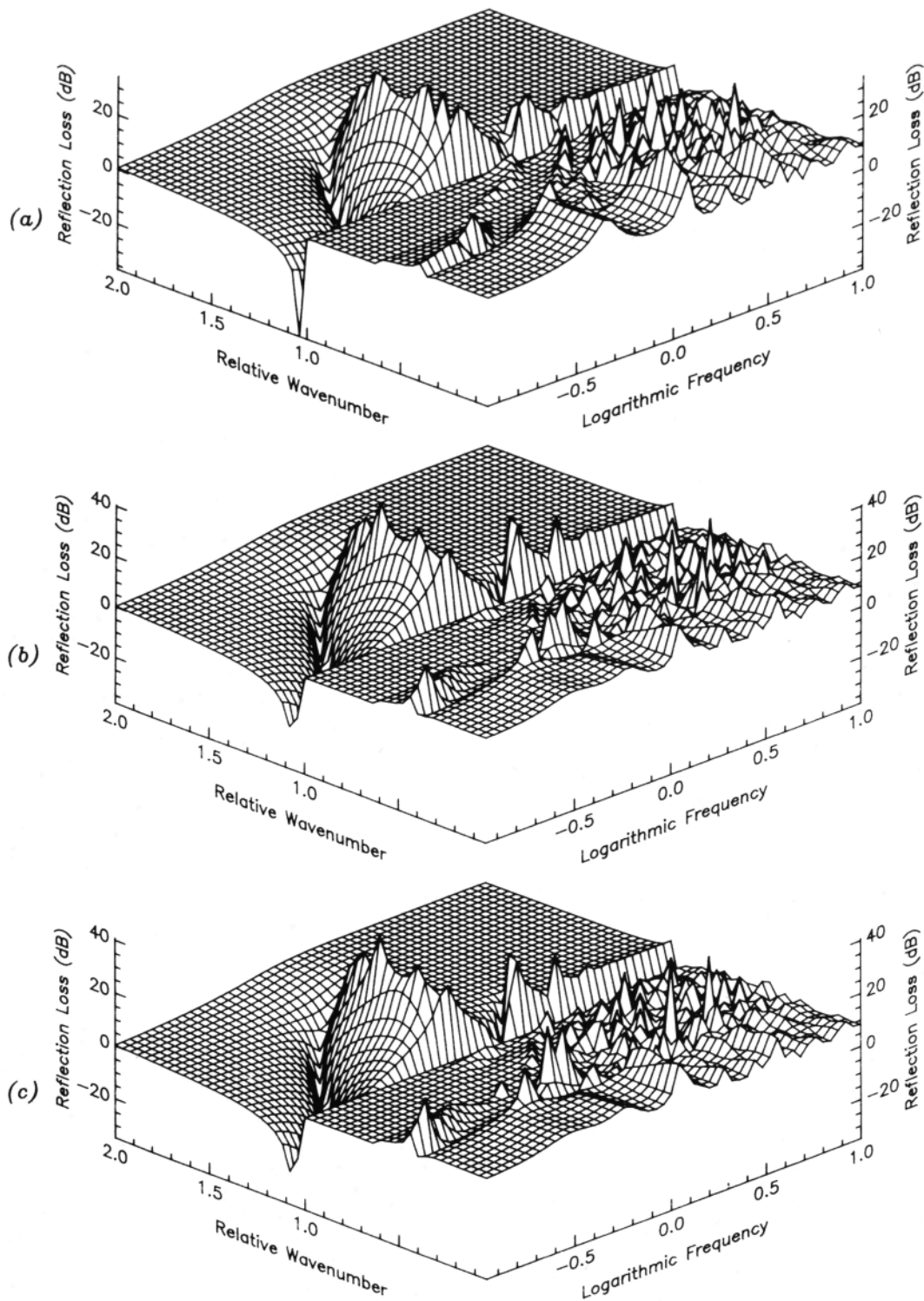


FIG. 13. Reflection loss for the K-model multilayered structure incorporating: (a) four layers, (b) five layers, and (c) six layers.

increases the interface wave is excited at the upper interface, and the effects associated with the lower interface disappear. At high frequencies (when the wave number is less than the thickness of the unconsolidated layer), high levels of reflection loss can occur in the inhomogeneous region as the result of total transmission between two liquid layers. The addition

of more sublayers adds some complication but the main features are still controlled by the basic elements described above.

Overall this analysis warns of the dangers of drawing conclusions about the angular and frequency dependence of the reflection loss on the basis of a limited number of

samples, and emphasizes the value of a three-dimensional analysis.

ACKNOWLEDGMENTS

This study was supported by a grant from the U.S. Office of Naval Research (N00014-92-J-1037).

- ¹H.P. Bucker, J.A. Whitney, G.S. Yee, and R.R. Gardner, "Reflection of low-frequency sonar signals from a smooth ocean bottom," *J. Acoust. Soc. Am.* **37**, 1037–1051 (1965).
- ²G.F. Fryer, "Reflectivity of the ocean bottom at low frequency," *J. Acoust. Soc. Am.* **63**, 35–42 (1978).
- ³F. Gilbert and G.E. Bachus, "Propagation matrices in elastic wave and vibration problems," *Geophysics* **31**, 326–332 (1966).
- ⁴S.R. Rutherford and K.E. Hawker, "The effects of density gradients on bottom reflection loss for a class of marine sediments," *J. Acoust. Soc. Am.* **63**, 750–757 (1978).
- ⁵K.E. Hawker and T.L. Foreman, "A plane-wave reflection loss model based on numerical integration," *J. Acoust. Soc. Am.* **64**, 1470–1477 (1978).
- ⁶P.J. Vidmar and T.L. Foreman, "A plane-wave reflection loss model including sediment rigidity," *J. Acoust. Soc. Am.* **66**, 1830–1835 (1979).
- ⁷P.J. Vidmar, "The effect of sediment rigidity on bottom reflection loss in a typical deep sea sediment," *J. Acoust. Soc. Am.* **68**, 634–638 (1980).
- ⁸P.J. Vidmar, "A ray path analysis of sediment shear-wave effects on bottom reflection loss," *J. Acoust. Soc. Am.* **68**, 639–648 (1980).
- ⁹P.J. Vidmar, "The dependence of bottom reflection loss on geoacoustic parameters of deep sea (solid) sediments," *J. Acoust. Soc. Am.* **68**, 1442–1453 (1980).
- ¹⁰P.J. Vidmar and R.A. Koch, "Shear-wave effects on propagation to a receiver in the substrate," in *Ocean Seismo-acoustics*, edited by T. Akal and J.M. Berkson, NATO Conference Series IV Marine Sciences, Proceedings of a SACLANT ASW Research Center Symposium, 10–14 June 1985 (Plenum, New York, 1986), pp. 149–159.
- ¹¹E.L. Hamilton, "Geoacoustic modeling of the sea floor," *J. Acoust. Soc. Am.* **68**, 1313–1340 (1980).
- ¹²E.L. Hamilton, "Acoustic properties of sediments" in *Acoustics and Ocean Bottom*, edited by A. Lara-Saenz, C. Ranz Cuierra, and C. Carbo-Fité (CSIS), Madrid (1987).
- ¹³F.B. Jensen and W.A. Kuperman, "Optimum frequency of propagation in shallow water environments," *J. Acoust. Soc. Am.* **73**, 813–819, (1983).
- ¹⁴P.J. Vidmar, "Gradient driven coupling between shear and compressional waves," *J. Acoust. Soc. Am.* **71**, 566 (1982).
- ¹⁵P.J. Vidmar, R.A. Koch, Jo.B. Lindberg, D.W. Oakley, and R. Pitre, "Acoustic bottom interaction: A review of recent work at ARL:UT," Applied Research Laboratories, University of Texas at Austin, TR-86-4 (1986).
- ¹⁶N.R. Chapman, "Modeling ocean bottom reflection loss measurements with the plane wave reflection coefficient," *J. Acoust. Soc. Am.* **73**, 1601–1607 (1983).
- ¹⁷N.R. Chapman, "Low frequency sound propagation in the ocean bottom," in Conference Proceedings, *Propagation and Noise in Underwater Acoustics*, Feb. 1990, edited by C.T. Tindle and G.E.J. Bold (Univ. of Auckland, Auckland, New Zealand, 1990), pp. 118–127.
- ¹⁸M.J. Buckingham, "Array gain of a broad vertical line array in shallow water," *J. Acoust. Soc. Am.* **65**, 148–161 (1979).
- ¹⁹D.M.F. Chapman, P.D. Ward, and D.D. Ellis, "The effective depth of a Pekeris ocean waveguide, including shear wave effects," *J. Acoust. Soc. Am.* **85**, 648–653 (1989).
- ²⁰Z.Y. Zhang and C.T. Tindle, "Complex effective depth of the ocean bottom," *J. Acoust. Soc. Am.* **93**, 205–213 (1993).
- ²¹A.C. Kibblewhite and K.C. Ewans, "Wave-wave interactions, microseisms and infrasonic ambient noise in the ocean," *J. Acoust. Soc. Am.* **78**, 981–994, (1988).
- ²²A.C. Kibblewhite, "Ocean noise spectrum below 10 Hz—mechanisms and measurements," in *Sea Surface Sound: Natural Mechanisms of Surface-Generated Noise in the Ocean*, edited by B. R. Kerman (Kluwer Academic, Dordrecht, 1988), pp. 337–359.
- ²³C.Y. Wu, "Wave-wave interactions and the infrasonic pressure field in the ocean," Doctoral dissertation, University of Auckland, New Zealand (1988).
- ²⁴A.C. Kibblewhite and C.Y. Wu, "The theoretical description of wave-wave interactions as a noise source in the ocean," *J. Acoust. Soc. Am.* **89**, 2241–2252 (1991).
- ²⁵A.C. Kibblewhite and C.Y. Wu, "An analysis of the ULF acoustic noise field in the ocean," in *Natural Physical Sources of Underwater Sound—Sea Surface Sound (2)*, edited by B.R. Kerman (Kluwer Academic, Dordrecht, 1993), pp. 189–202.
- ²⁶A.C. Kibblewhite and C.Y. Wu, "A study of reflection loss. I. Involving a porous layer and a demonstration of the Biot slow wave," *J. Acoust. Soc. Am.* **96**, 2981–2992 (1994).
- ²⁷M.A. Biot, "General theory of three-dimensional consolidation," *J. Appl. Phys.* **12**, 155–164 (1941).
- ²⁸M.A. Biot, "Theory of propagation of elastic waves in a fluid-saturated porous solid: I. Low-frequency range," *J. Acoust. Soc. Am.* **28**, 168–178 (1956).
- ²⁹M.A. Biot, "Theory of propagation of elastic waves in a fluid-saturated porous solid. II. Higher frequency range," *J. Acoust. Soc. Am.* **28**, 179–191 (1956).
- ³⁰M.A. Biot, "Generalized theory of acoustic propagation in porous dissipative media," *J. Acoust. Soc. Am.* **34**, 1254–1264 (1962).
- ³¹M.A. Biot, "Mechanics of deformation and acoustic propagation in porous media," *J. Appl. Phys.* **33**, 1482–1498 (1962).
- ³²R.D. Stoll and G.M. Bryan, "Wave attenuation in saturated sediments," *J. Acoust. Soc. Am.* **47**, 1440–1447 (1969).
- ³³R.D. Stoll, "Acoustic waves in saturated sediments," in *Physics of Sound in Marine Sediments*, edited by L.D. Hampton (Plenum, New York, 1974), pp. 19–39.
- ³⁴R.D. Stoll, "Acoustic waves in ocean sediments," *Geophysics* **42**, 715–725 (1977).
- ³⁵R.D. Stoll, "Theoretical aspects of sound transmission in sediments," *J. Acoust. Soc. Am.* **68**, 1341–1350 (1980).
- ³⁶R.D. Stoll, "Marine sediment acoustics," *J. Acoust. Soc. Am.* **77**, 1789–1799 (1985).
- ³⁷R.D. Stoll and T.K. Kan, "Reflection of acoustic waves at a water-sediment interface," *J. Acoust. Soc. Am.* **70**, 149–156 (1981).
- ³⁸R.D. Stoll, *Sediment acoustics*, Lecture Notes in Earth Sciences, edited by S. Bhattacharji, G.U. Friedman, H.J. Neugebauer, and A. Sesslacher (Springer-Verlag, New York, 1989).
- ³⁹H. Schmidt and F.B. Jensen, "A full-wave solution for propagation in multilayered viscoelastic media with application to Gaussian beam reflection at fluid–solid interfaces," *J. Acoust. Soc. Am.* **77**, 813–825 (1985).
- ⁴⁰G.V. Frisk, "Inhomogeneous waves and the plane wave reflection coefficient," *J. Acoust. Soc. Am.* **66**, 219–233 (1979).
- ⁴¹A.O. Williams, Jr., "Hidden depths—Ignorance about ocean bottoms," *J. Acoust. Soc. Am.* **59**, 1175–1179 (1976).